CCR2 Influences T Regulatory Cell Migration to Tumors and Serves as a Biomarker of Cyclophosphamide Sensitivity

Pierre-Louis Loyher, Juliette Rochefort, Camille Baudesson de Chanville, Pauline Hamon, Géraldine Lescaille, Chloé Bertolus, Maude Guillot-Delost, Matthew F. Krummel, François M. Lemoine, Christophe Combadiere, et al.

CCR2 influences T regulatory cell migration to tumors and serves as a biomarker of cyclophosphamide sensitivity.

Pierre-Louis Loyher[1], Juliette Rochefort[1], Camille Baudesson de Chanville[1], Pauline Hamon[1], Géraldine Lescaille[1], Chloé Bertolus[1,2], Maude Guillot-Delost[1], Matthew F Krummel[3], François M. Lemoine[1], Christophe Combadière[1] and Alexandre Boissonnas[1*]

[1] Sorbonne Universités, UPMC Université Paris 06 UMR_S1135, Institut universitaire de cancérologie (IUC), Inserm U1135, CNRS ERL8255, Centre d'Immunologie et des Maladies Infectieuses, 91 Boulevard de l'Hôpital, F-75013, Paris, France.
[2] Department of Maxillofacial surgery, AP-HP, Hôpital Pitié-Salpêtrière, Paris, F-75013 France.
[3] Department of Pathology, University of California San Francisco, San Francisco, California, USA

Running Title: CCR2 controls tumor T regulatory cells

Keywords: Chemokine, Immunossuppression, Cancer Immunology, T regulatory cells, Chemotherapy

Notes:
Corresponding author:
Alexandre Boissonnas
e-mail: alexandre.boissonnas@upmc.fr
CIMI U1135 91 Bd de l'hôpital 75013 Paris, France
Tel: +33140779840 fax: +33140779734

Conflict of Interest: There is no conflict of interest
Word count: 5,990
Number of Figures and Tables: 7 figures, no table, 4 supplement figures, 1 supplemental document (methods and figure legends).

Financial support:

The research leading to these results received funding from the European Community's Seventh Framework Programme (FP7/2007-2013) under grant agreement n° 304810 – RAIDs, from Inserm, from la "Ligue contre le cancer", from "Association pour la Recherche sur le Cancer". PH is funded by la "Ligue contre le cancer".

Abstract

The CCL2 chemokine receptor CCR2 drives cancer by mediating recruitment of monocytes and myeloid-derived suppressor cells to the tumor microenvironment. In this study, we extend the significance of CCR2 in this setting by identifying a new role for it in mediating recruitment of $CD4^+$ T regulatory cells (Treg). Following tumor initiation, an expanded population of $CCR2^+$ Tregs required CCR2 expression to traffic between draining lymph nodes (dLN) and the tumor. This Treg subset was enriched in the fraction of tumor antigen-specific cells in the dLN, where they displayed an activated immunosuppressive phenotype. Notably, low-dose cyclophosphamide treatment preferentially depleted $CCR2^+$ Treg, enhancing priming of tumor-specific $CD8^+$ T cells. In the MMTV-PyMT transgenic mouse model of breast cancer and in oral squamous cell carcinoma patients, tumor development was associated with decreased blood frequency and inversely increased tumor frequency of $CCR2^+$ Tregs. Our results define a novel subset of $CCR2^+$ Treg involved in tumoral immune escape, and they offer evidence that this Treg subset may be preferentially eradicated by low-dose cyclophosphamide treatment.

Introduction

Chemokine-chemokine receptor interactions play major roles in the shaping of the tumor microenvironment (TME). These interactions can induce the differential recruitment of immune cells and by this mean turn the TME into an immunosuppressive site(1,2). CCR2, a chemokine receptor highly expressed by inflammatory monocytes, is crucial for the recruitment of the latter from the bone marrow to inflamed tissues(3) but also displays chemotactic properties for T-cells(4,5). Secretion of the major CCR2 ligand (CCL2) by both the tumor and tumor-stromal cells is common in many tumor types in both human and mouse models(6,7). For these reasons the CCR2-CCL2 axis is an important mechanistic marker of tumor development(8) and can also predict clinical benefit after cancer therapy(6). Beyond tumor-associated myeloid cells, regulatory T-cells (Tregs) have a well-established role in promoting tumor tolerance and represent an obstacle to efficient T-cell-based anti-tumor immunotherapy(9-11). Suppression of anti-tumor effector functions of both $CD4^+$ helper T-cells and cytotoxic $CD8^+$ T-cells by Tregs can occur through various cell-to-cell or soluble mechanisms(12) both in draining lymph nodes (dLN)(13) or in the tumor itself(9). A better understanding of the mechanisms involved in Tregs trafficking and accumulation within the TME is thus needed.

Tregs display different homing properties and their appropriate compartmentalization is crucial for their in vivo activity(14,15). Following thymus emigration, Tregs can enter secondary lymphoid organs in a CCR7, CD62L dependent fashion. This lineage can be maintained throughout time by further recruitment or by continuous self-renewal(16). Activation and antigen priming in secondary lymphoid organs promote down-regulation of CCR7 and CD62L while other memory/effector type trafficking receptors may be upregulated to allow Tregs to migrate into non-lymphoid or inflamed

tissues(14,17-19). To date, few chemokine receptors have been associated with the tumor homing properties of Tregs, though a role for CCL22 in the recruitment of $CCR4^+$ Tregs into human ovarian and/or breast cancer has been described(20-22).

CCL2 is described as a pro-inflammatory cytokine, but contradictory functions have been observed in the absence of CCR2 in non-infectious inflammatory models(23,24). A dual role for CCR2 was described in a model of arthritis because a subset of highly suppressive Treg, expressing CCR2, expanded during the course of the disease(24). The chemokine receptors CCR2, CCR4 and CCR5 and P-and E-selectins were all necessary to ensure efficient homing of Tregs to a graft tissue(25). Finally, in a model of delayed-type hypersensitivity reaction, antigen-specific Tregs required CCR2 to migrate toward the antigen site(26). All together, these findings support a role for CCR2 in the homing of activated Tregs to an inflamed site.

We therefore hypothesized that CCR2 expression on Tregs might play a central role in tumor context. Herein, we studied the role of CCR2 on the compartmentalization and the dynamic of Tregs in different tumor models, as well as, human oral squamous cell carcinoma (OSCC). We showed that $CCR2^+$ Tregs represent a discrete subset that is highly important for suppressing anti-tumor responses. Finally, we observed a selective depletion of this subset by low-dose cyclophosphamide (CP) which provides new interpretation in the Treg mediated effect of CP treatment.

Material and Methods

Ethical statement

All experiment protocols were approved by the French animal experimentation and ethics committee and validated by "Service Protection et Santé Animales, Environnement" with the number A-75-2065 for tumor experiments and A-75-1315 for parabiosis experiments. Human samples were obtained after informed written consent according to local ethic committee authorization.

Human tissue and blood samples

Blood (n=30) and tumors (n=14) samples from patients with primary OSCCs (3 at stage 1, 4 at stage 2, 1 at stage 3, 26 at stage 4) obtained during surgical resection (Department of maxillo-facial surgery, Pitié-Salpêtrière Hospital; Paris, France). Gingival tissues (n=10) were collected from healthy subjects undergoing preventive wisdom tooth extraction (Odontology department, Pitié-Salpêtrière Hospital; Paris, France). Control blood samples (n=42) were obtained from volunteer healthy donors (Etablissement Francais du Sang, Paris, France). The male to female ratio was 1.7:1 for OSCC blood patients (mean age 60.8±10 years); 1.9:1 (mean age 51.6±18.1 years) for control blood and 2.5:1 for tumors patients (mean age 62.5±8.9 years); 1.5:1 for gingival tissues (mean age 40.2±18 years).

Mice

C57BL/6 (10-14 weeks) were obtained from JANVIER LABS (Le Genest-Saint-Isle, France). C57BL/6 *Rag2*$^{-/-}$ TCR (Vα2, Vβ5) transgenic mice (OT1) were crossed to CD45.1 C57BL/6 (Animalerie centrale, Institut Curie, Paris) to obtain OTI CD45.1 mice. Foxp3-EGFP transgenic mice, *Ccr2*$^{-/-}$, *Ccr1*$^{-/-}$, *Ccr5*$^{-/-}$, *D6*$^{-/-}$ and Foxp3-EGFP X *Ccr2*$^{-/-}$

mice were bred in the Animal facility (Centre d'Exploration Fonctionelle, Pitié-Salpétrière, Paris). MMTV PyMT-P2A-mCherry-P2A-OVA (PyMT-ChOVA) mice(27) were crossed with *Ccr2*$^{-/-}$ mice. *Ccr2*$^{rfp/+}$ mice were kindly provided by Israel Charo (Gladstone Institute, San Francisco)(28).

Parabiosis

C57BL6 female host parabionts were generated with Foxp3-EGFP X *Ccr2*$^{-/-}$ females, injected with MCA-OVA tumor cells 15 days after surgery to allow establishments of blood chimerism and analyzed 10 days later. The Treg chimerism was evaluated by determining the percentage of EGFP-expressing *Ccr2*$^{-/-}$ Treg out of total Treg intracellularly stained with Foxp3 antibody.

Cells

The MCA-OVA cell line (kindly provided by Dr. C. Théry, Institut Curie, Paris France) is stably transfected with a plasmid encoding for soluble ovalbumin (OVA)(29). MCA-OVA cell line was cultured in Dulbecco's modified Eagle's medium with GlutaMAX supplemented with antibiotics and 10% fetal calf serum. CD8^{+} OT1 T-cells (specific for $OVA_{257-264}$ peptide in a H2-K^{b} context) were obtained from lymph nodes of OT1 *Rag2*$^{-/-}$ mice (herein called OT1 T-cells, with purity between 94% and 98%).

Tumor engraftment and mice anti-tumor treatment

Protocols from(30,31) were strictly reproduced. Briefly, MCA-OVA cells ($2x10^{5}$) were injected subcutaneously in the flank of mice. Tumor size was measured twice a week using a caliper, $V = L \times l \times (L + l)/2$. Low-dose chemotherapy was performed 7 days after tumor inoculation by a single intraperitoneal injection of cyclophosphamide

(Sigma-Aldrich, Saint-Quentin Fallavier, France) diluted in phosphate-buffered saline (PBS) at 100mg/kg. Adoptive T-cell transfer was performed on day 10 after tumor inoculation by intravenous (i.v) injection of $5x10^6$ freshly harvested OTI T-cells.

ELISA

Plasma, tumor and lymph node tissues were harvested on indicated days, stored in PBS at -80°C, thawed and centrifuged to obtain tissue homogenates. Murine CCL2 ELISA was performed using Quantikine ELISA Mouse Immunoassay kits (Bio-techne) following the manufacturer's protocol.

Flow cytometry

Phenotypic characterization of all murine cell populations was performed using either a FACS Canto II or FACS LSRFortessa (Becton Dickinson, Franklin Lakes, NJ) for acquisition. For analysis, FlowJo software (Tree Star Inc, Ashland, OR) was used. MCA-OVA tumors, MMTV-PyMT primary mammary tumors (3-4 days after detection by palpation) and dLN (axillary) were entirely mashed in PBS with 0.5% Bovine serum albumin/2mM EDTA (FACS Buffer) and filtered using 70-µm cell strainer (BD Biosciences, San Jose, CA). Blood was drawn and lysed in RBC lysis buffer containing 0.15M NH4Cl, 0.01mM KHCO3 and 0.1mM EDTA. Surface staining was performed by incubating 50µl of cell suspension (1/10th of the total) with 1µg/ml purified anti CD16/32 (2.4G2; BD Biosciences) for 10min at 4°C and for an additional 20min with appropriate dilution of specific surface antibodies. Dead cell were excluded using LIVE/DEAD Fixable stain (Life technologies) according to manufacturer's instructions. Forward- and side-scatter parameters were used for doublets exclusion. After incubation, cell suspensions were washed once in FACS Buffer. For $CD4^+$ tumor antigen-specific T-

cells analysis, cells were stain with the T-select MHC Class II mouse tetramer I-A^b $OVA_{323-339}$ Tetramer-PE (MBL International Corporation) prior to surface staining according to manufacturers' instructions. CCL2 binding assay was achieved as previously described(32). Briefly, after surface staining, cells were incubated in the dark for 45min at 37°C in RPMI medium with GlutaMAX containing 25nM murine $CCL2^{AF647}$(Almac Sciences, Craigavon, UK). Cells were then washed in FACS Buffer. In some experiments cells were pre-incubated with 10µM recombinant human rhCCL2 chemokine (Peprotech, Neuilly-sur-seine, France) at 37°C for 45min. For DNA content analysis, cells were incubated with 16µM Hoechst in a final volume of 500µL of FACS buffer with shaking at 37°C for 45min prior to surface staining and washed with 3mL of FACS buffer. For intracellular OTI IFN-γ staining, cell suspensions were re-stimulated ex vivo with 1µM $OVA_{257–264}$ for 3 hours at 37°C in the presence of 5µg/ml Brefeldin A. For IL-10 staining, cells were pre-incubated for 6 hours with cell activation cocktail with Brefeldin A according to manufacturers' instructions (BioLegend). After surface staining, cells were fixed in 4% paraformaldehyde (PFA) for 20min, washed twice in perm/washsolution (BD Biosciences), incubated 10 min with 1µg/ml purified anti-CD16/32 in perm/wash at room temperature and incubated for 30min in perm/wash in the presence of anti–IFN-γ or anti-IL-10. For intracellular staining the Foxp3/Transcription Factor Staining Buffer Set, anti-Foxp3 and anti-Ki-67 (eBioscience) were used according to manufacturers' instructions. Samples were washed in FACS buffer before acquisition. Calculation of absolute numbers of different cell populations was performed by adding in each vial a fixed number (10,000) of nonfluorescent 10-µm polybead carboxylate microspheres (Polysciences, Niles, IL) according to the formula: Nb of cells=(Nb of acquired cells×10,000)/(Nb of acquired

beads). The number of cells obtained for each sample was extrapolated to the whole organs.

Cell suspensions from human tumor and gingival samples were obtained after non-enzymatic digestion using Cell Recovery Solution (Corning, Avon, France) at 4°C for 1 hour. After filtering, washing and counting, cells were stained with Fixable Viability Dye eFluor780 (eBioscience) at 2-8°C for 30min. Cells from tissues and whole blood were stained with directly labeled surface antibodies at 4°C during 20min, and permeabilized with Foxp3/TFs Staining Buffer Set (eBioscience) for intracellular staining, according to manufacturer's instructions. After staining, whole blood was lysed to eliminate red blood cells. Acquisition and data analyses were performed using LSRII flow cytometer (Becton Dickinson) and FlowJo software (TreeStar, Ashland, OR, USA).

In vivo proliferation assay

CD45.1 OTI T-cells were incubated for 10min at 37°C in PBS with 5mM carboxyfluorescein diacetate succinimidyl ester (CFSE; Molecular Probes, Invitrogen, Cergy Pontoise, France). Cells (5×10^6) were injected in PBS into CD45.2 tumor-bearing or tumor-free mice. After 4 days, the frequency and number of OTI T-cells that had performed more than three divisions (defined as highly divided) in dLN and tumor were measured while gating on $CD45.1^+CD8^+$ cells.

Supplemental information

Additional information can be found in Supplementary Material and Methods.

Results

CCR2 expression on Tregs is required for tumor-infiltration

We first examined the impact of CCR2 invalidation on tumor growth and on the compartmentalization of Tregs in mice injected subcutaneously with the methyl-cholanthrene induced, ovalbumin expressing, tumor cell line (MCA-OVA). We previously showed the importance of Treg in limiting anti-tumor $CD8^+$ T-cell responses in this model(30). In *Ccr2*$^{-/-}$ mice, tumor growth was slightly reduced by day 13 after tumor inoculation, as compared to wild type (WT) mice. These differences in tumor size became significant on day 20 and were then sustained throughout the monitoring period **(Figure 1A)**. In keeping with a role of the CCR2/CCL2 axis in tumor development, the CCR2 chemokine CCL2 was detected in MCA-OVA cell line supernatants **(Figure 1B)** and was found to increase in inoculated tumor from day 7 to day 19 **(Figure 1C)**. In WT mice, the percentage of tumor-infiltrating Tregs ($CD25^+Foxp3^+$) among $CD4^+$ cells increased between day 7 and day 13. In *Ccr2*$^{-/-}$ mice, the frequency of tumor-infiltrating Tregs was similar on day 7 compared to WT mice but they failed to further accumulate **(Figure 1D and supplemental 1A)** The absolute count of Treg per mg of tumor increased between day 7 and day 10, stabilized between day 10 and day 13 in WT mice but diminished in proportion to tumor weight in *Ccr2*$^{-/-}$ mice **(supplementary figure 1B)**. On the other hand, the numbers of intra-tumor conventional $CD4^+CD25^-Foxp3^-$ helper T-cells (Th) were not significantly reduced by CCR2 deficiency **(supplementary figure 1C)**. In the draining lymph node (dLN), the frequency of Tregs among $CD4^+$ cells was similar **(Figure 1D).** Because the number of Tregs increased similarly with time in WT and *Ccr2*$^{-/-}$ mice, we excluded that the defect of tumor infiltration was due to a defect of Tregs amplification in the dLN. A significantly higher accumulation of Tregs but not Th in the dLN of *Ccr2*$^{-/-}$ mice was

even observed on day 13 **(supplemental Figure 1D and E)**. Thus, we uncovered a role of the CCL2/CCR2 axis in the preferential tumor recruitment of Tregs compared to Th cells over time.

To confirm that the defect of Treg infiltration into the tumor in the absence of CCR2 was intrinsic to Tregs, we performed parabiosis experiment between WT and Foxp3-EGFP *Ccr2*$^{-/-}$ mice **(Figure 1E)**. The proportion of EGFP^{+} *Ccr2*$^{-/-}$ Tregs among total Tregs in the dLN and tumor was determined on day 10 after tumor injection in both parabiont hosts. In the dLN, the absence of CCR2 did not seem to affect Tregs expansion and distribution. In contrast, EGFP^{+} *Ccr2*$^{-/-}$ Tregs that migrated to the tumor tissue represented only 19.8±6.8% of total Tregs in WT host and 20.1±7% of total Tregs in *Ccr2*$^{-/-}$ host **(Figure 1F-G)**. These results indicate that CCR2 expression by Tregs is required for their accumulation to the tumor site.

A transient increased in CCL2 protein level was detected in the dLN on day 7 and day 10 but resumed to basal value by day 13 **(Supplemental figure 2A)**. Plasma CCL2 protein level was also slightly increased after MCA-OVA inoculation at all the time point analyzed **(Supplemental figure 2B)**. We therefore speculated that the CCR2/CCL2 axis could also locally regulate Tregs migration in the dLN. In situ analysis of Tregs dynamic by real-time imaging showed increased motility in tumor dLN compared to non-dLN (mean velocity of 7.3±4.6µm/min vs 2.9±3µm/min respectively) **(Supplemental figure 2C-D)**. Tregs displayed various migratory behaviors ranging from highly motile to completely arrested. In WT mice, up to 36% of Foxp3^{gfp} Tregs were highly motile never making significant arrest during their track **(Supplemental figure 2E)**. In *Ccr2*$^{-/-}$ mice, the mean velocity of FoxP3^{gfp} Tregs in the dLN was slightly reduced compared to WT mice (6±4.3µm/min) **(Supplemental figure 2D)** and the proportion of highly motile Tregs dropped to 12% **(Supplemental figure 2E)**.

We could not detect any significant differences in the absolute count of 4 different subsets of antigen-presenting cells (APC) between WT and *Ccr2*$^{-/-}$ mice that could affect Tregs interactions or displacement and account for the defect of migration **(Supplementary Figure 2F-G)**.

These results indicated that CCR2 contributed to increasing the dynamic of Tregs within the dLN and might reflect Tregs emigration from the dLN toward the tumor.

CCR2^{+} Tregs accumulate during tumor development

We next investigated whether Tregs express the CCR2 receptor at their surface. CCR2 staining using the antibody that labeled inflammatory monocytes was not detected on Treg. CCR2 is the best known receptor for the chemokine CCL2 and presents high affinity for this chemokine. Using the CCR2 ligand, conjugated with Alexa-647 dye (CCL2^{AF647}) as previously done(32), we revealed functional surface CCR2 receptor expression in both blood inflammatory monocytes and Tregs **(supplementary Figure 3A).** A significant and distinct fraction of Tregs binds the chemokine in the tumor, blood, and dLN **(Figure 2)**. This binding was almost completely abrogated in *Ccr2*$^{-/-}$ mice and in the presence of competitive non-labeled CCL2 **(supplementary Figure 3B)**, but was similar in CCR1, CCR5 and D6-deficient mice, the three other receptors that have been shown to bind CCL2 with lower affinity **(supplementary Figure 3C)**. CCL2-binding was specifically detected on RFP^{+} Tregs reporting *Ccr2* transcription **(supplementary Figure 3D)**. CCL2 binding was assessed in both Th and Treg compartments and the proportion of cells binding the chemokine in WT mice but not in *Ccr2*$^{-/-}$ were therefore considered to be CCR2^{+} T-cells. At steady state, 8.8±4.9% of Tregs were CCR2^{+} in the dLN, whereas less than 2% of Th cells bound CCL2 (**Figure 2A)**. The proportion of CCR2^{+} Tregs peaked to 21.3±8.4% on day 10 and subsequently

felt to 16.5±2.3% on day 19. In the blood, the percentage of CCR2$^+$ Tregs was 10.9±5.8% at steady state, increased up to 23.5±5.4% on day 10 and dropped to 17.27±3.4% on day 19 **(Figure 2B)**. In contrast, the proportion of CCR2$^+$ Th did not significantly increase in those tissues over time **(Figure 2A-B)**. In the tumor, the proportion of CCR2$^+$ Tregs was higher compared to dLN and blood but remain stable over time (from 48.1±17.9% on day 7, to 58.2%±13.7 on day 19) The proportion of CCR2$^+$ tumor-infiltrating Th still remained lower **(Figure 2C)**. Finally, CCR2$^+$ Tregs represented both distinct and differentially overlapping subsets with the CCR4$^+$ CCR5$^+$ and CCR6$^+$ Tregs in the dLN and these CCR2$^+$ Tregs were preferentially enriched within the tumor compared to the other subsets. Notably, the proportion of CCR2$^+$ Treg co-expressing CCR4 and CCR6 was lower in the tumor compared to dLN, whereas the one co-expressing CCR5 remained similar **(supplementary Figure 3E)**.

We concluded that the CCR2$^+$ Treg fraction sequentially increased in the dLN and the blood during the early steps of tumor growth while it was constantly highly represented among tumor infiltrating Tregs. Overall our results suggested that CCR2 represents a major Treg homing receptor in tumor context.

CCR2$^+$ Tregs are activated, IL-10 producing and tumor-antigen specific cells

In order to better characterize CCR2$^+$ Tregs, we compared the phenotype of CCR2$^+$ and CCR2$^-$ Tregs in the dLN and in the tumor. In the dLN, CCR2$^+$ Tregs displayed an activated phenotype, expressing higher levels of CD44, lower levels of Ly6C and CD62L as compared to CCR2$^-$ Tregs. In the tumor, CCR2$^+$ and CCR2$^-$ Tregs were all CD44^{high}, CD62L^{low} and Ly6C^{low} **(Figure 3A)**. In addition, CCR2$^+$ Tregs were the cells with the highest capacity to produce IL-10 after phorbol 12-myristate 13-

acetate (PMA)-Ionomicyne stimulation compared to CCR2$^-$ Tregs, but also compared to CCR2$^+$ and CCR2$^-$ Th lymphocytes **(Figure 3B)**.

Accordingly, the CCR2$^+$ Treg subset in the dLN was cycling more than the CCR2$^-$ Treg subset as shown by Hoechst and Ki-67 staining **(Figure 3C-D)**.

CD73 and CD39 expression on Tregs have been previously associated with strong immunosuppression(33). CD73 expression was similar in CCR2$^+$ and CCR2$^-$ Tregs but CD39 expression was greater in the former **(Figure 3E)**. Finally, staining with OVA-323-339 MHCII tetramer (I-Ab OVA-323-339) revealed that tumor-antigen specific Tregs were more restricted to the CCR2$^+$ subset **(Figure 3F)**. We concluded that CCR2$^+$ Tregs represent proliferating tumor-activated-Tregs with a high immunosuppressive activity.

CCR2$^+$ Tregs are preferentially depleted by low-dose CP treatment

Low-dose of cyclophosphamide (CP) has been shown to specifically deplete Tregs, thereby enhancing anti-tumor T-cells priming and proliferation(34,35). We thought to analyze the impact of this alkylating agent on dLN CCR2$^+$ Tregs.

As expected, after one single low-dose of CP (100mg/kg) on day 7, the percentage of Tregs in the dLN was reduced by 25% on day 10 and recovered on day 13 in WT mice. The percentage of Tregs remained barely affected in *Ccr2*$^{-/-}$ mice **(Figure 4A)**. The depletion observed in WT mice preferentially affected CCR2$^+$ Tregs. Indeed, the absolute number of CCR2$^+$ Tregs gradually decreased from day 7 to day 10 (93% depletion) whereas CCR2$^-$ Tregs were less affected (52% depletion). For both subsets, Treg recovery occurred within 3 days **(Figure 4B)**. CP sensitivity was selective to the CCR2$^+$ Tregs compared to CCR4$^+$, CCR5$^+$ and CCR6$^+$ Tregs emphasizing the preferential targeting of the CCR2$^+$ subset (**Figure 4C)**. The frequency of cycling Tregs

among total Treg of the dLN confirmed that CP treatment preferentially ablated proliferating Tregs **(Figure 4D)**. Comparative cell cycle analysis in the dLN on day 8 and day 13, first revealed that the proportion of Tregs but not Th cells engaged in cell cycle is higher in WT mice compared to *Ccr2*$^{-/-}$ mice**.** Nevertheless, the absolute numbers of cycling Tregs are identical arguing that non-cycling Tregs accumulate in the dLN of *Ccr2*$^{-/-}$ mice **(Supplementary Figure 4)**. We conclude that CCR2^{+} Tregs are preferentially targeted by low-dose CP due to their higher activating and proliferating state, and that in the absence of CCR2, non-cycling Tregs are retained in the dLN leading to lower depletion after CP treatment.

Low-dose CP fails to enhance the priming of OT-1 in the dLN of *Ccr2*$^{-/-}$ mice.

We previously showed that low-dose CP treatment transiently enhances anti-tumor CD8^{+} T-cell response against MCA-OVA tumor(31). In order to assess whether the reduced Treg depletion in *Ccr2*$^{-/-}$ mice treated with low-dose CP has a functional impact, we adoptively transferred naive OT-1 CD8^{+} cytotoxic T-cells 3 days after CP treatment and analyzed 3 days after transfer cell proliferation and IFN-γ production in the dLN. In CP treated WT mice, the proliferation rate of OT-1 cells was improved by 2.5 fold whereas OT-1 cell count was not significantly changed in *Ccr2*$^{-/-}$ mice. The percentage of IFN-γ producing OT-1 was also increased in WT CP treated mice but not in *Ccr2*$^{-/-}$ mice **(Figure 5A-B)**. Accordingly, the therapeutic combination did yield a significant reduction in tumor growth from day 18, when compared to mice treated with low-dose CP alone, but this beneficial effect was completely lost in *Ccr2*$^{-/-}$ mice **(Figure 5C)**. All together these results indicate that preferential depletion of CCR2^{+} Tregs is associated with increased priming of tumor specific CD8^{+} T-cells. On the other hand,

in *Ccr2*$^{-/-}$ mice, where Tregs are not as effectively depleted, low-dose CP failed to enhance the priming of tumor-specific CD8^{+} T-cells.

CCR2^{+} Tregs accumulate within spontaneous mammary carcinoma and are preferentially depleted by low-dose CP

We next evaluated whether the CCR2^{+} Treg subset expansion could be applicable to a less inflammatory and a more progressive tumor model. CCL2^{AF647} was also used to stain CCR2^{+} CD4^{+} T-cells in the spontaneous Cherry-OVA PymT mammary carcinoma model in which tumor apparition occurs at 23±2.1 weeks of age. Consistent with the results in the MCA-OVA tumor model, CCL2 binding defined a higher proportion of CCR2^{+} Treg compared to Th in the dLN, blood and tumor**.** PymT mice were treated with either PBS or low-dose CP once tumor nodules were palpable and frequencies of CCR2^{+} Tregs and Th cells were monitored 3 days after treatment. Similarly to the observations made in the MCA-OVA model, low-dose CP led to a preferential depletion of CCR2^{+} Tregs in the different compartments **(Figure 6A-C)**. Additionally we found that a lower percentage of CCR2^{+} Tregs in the blood and a higher percentage of CCR2^{+} Tregs in the tumor correlated with an earlier onset of tumor development **(Figure 6D)**.

CCR2^{+} Tregs accumulate within human OSCC

Finally, we examined the expression of CCR2 in Tregs (CD4^{+}CD25^{+}Foxp3^{+}CD127^{-}) and Th cells (CD4^{+}CD25$^{-/low}$Foxp3^{-}) cells isolated from blood and tumors of OSCC patients and compared to healthy blood donors and non-tumor gingival tissues from patients undergoing wisdom tooth extraction. Compared to the mouse, the human anti-CCR2 antibody did provide a good signal quality on T-cells**.** The specificity of CCR2

staining was confirmed by pre-incubating the cells with unlabelled CCL2 chemokine which inhibited the binding of the CCR2 antibody and allowed to define our gating for $CCR2^+$ T-cells **(Figure 7A)**. Although, the proportions of $CCR2^+$ Th in the blood were similar between OSCC patients and control blood (13.9±4.9%, 14.1±6.7%), the percentage of $CCR2^+$ Treg was significantly decreased in patients (10.9±4 %) as compared to healthy donors (17.1±5.3%) **(Figure 7B)**.The frequency of $CCR2^+$ Th cells was also similar between tumor tissue and healthy gingiva. However, the percentage of $CCR2^+$ Treg was increased to 38.6±6.5% in tumor tissues as compared to healthy gingival (28.1±7.9). In conclusion, in OSCC patients we observed a reduced frequency of circulating $CCR2^+$ Treg while they accumulated in the tumor microenvironment.

Discussion

Chemokine receptor mediated immune cell migration is usually achieved through combinatorial expression of multiple chemokine receptors(1). So far, most studies on the direct role of the chemokine CCL2 and its main receptor CCR2 have focused on myeloid cells because of their higher CCR2 expression. However, tumor derived CCL2 was shown to be sufficient to mediate the tumor tropism of adoptively transferred T-cells(36). Reduction of intra-tumor Tregs was observed in previous study following CCL2 blockade(37), but the direct role of this axis in mediating the tumor homing of Treg has not been studied in depth.

We investigated whether the CCL2 chemokine could be also used by Tregs for their homing toward solid tumors in vivo. The reduction of tumor growth in *Ccr2*$^{-/-}$ mice was associated with a drastic reduction in both the number and percentage of Tregs inside the tumor. Parabiosis experiments to track the fate of *Ccr2*$^{-/-}$ Tregs in analogous microenvironments suggest that CCR2 expression on Tregs is required for the migration toward the tumor of at least 50% of Tregs, representing approximately the fraction of CCR2^{+} Tregs within the tumor. The CCR2^{+} Treg subset started to expand in the dLN concomitantly with the appearance of differences in tumor size between WT and *Ccr2*$^{-/-}$ mice, as well as the tumor-infiltration of CCR2^{+} Tregs. These observations suggest the induction of two distinct, CCR2-independent and CCR2-dependent, phases of Tregs recruitment. The CCR2^{+} Treg subset phenotype was consistent with one of activated Treg, highly cycling and immunosuppressive compare to CCR2^{-} Tregs. Additionally, the dynamic behavior of endogenous Tregs was affected by CCR2 deficiency in the dLN but not in non-dLN. Indeed, we found a significant enrichment of tumor-antigen specific Tregs in the CCR2^{+} versus CCR2^{-} fraction. As a result, CCR2 up-regulation by Tregs might follow tumor-induced T-cell activation.

The spontaneous PyMT model relates more to a chronic inflammatory state, where tumors slowly develop compared to the more acute and aggressive inoculated cell lines(38). In this model, Tregs ablation was demonstrated to reduce both primary and metastatic tumor progression though increased IFN-γ production(39). In the same line, increased frequency and suppressive activity of Tregs were associated with advanced stages in OSCC patients(40-42). In both the Pymt model and human OSCC patients we observed a lower blood frequency and higher tumor frequency of $CCR2^+$ Tregs compared to healthy controls. In the Pymt model, the onset of tumor apparition correlated with increased $CCR2^+$ Tregs blood frequency but decreased tumor frequency. In this case, increased recruitment of $CCR2^+$ Tregs to the tumor might explain the lowering of the blood frequency and suggests that intra-tumoral $CCR2^+$ Tregs favor immune suppression and accelerate tumor escape. In the MCA model, both blood and dLN $CCR2^+$ Tregs frequency peaked on day 10 post tumor inoculation and subsequently reduced. This observation might reflect the early establishment of immune tolerance after tumor inoculation that is difficult to observe during spontaneous long-term tumor development in mice and humans.

Preferential depletion of Treg versus non-Treg compartment by the chemotherapeutic agent cyclophosphamide allows for the induction of an improved response to immunotherapies in pre-clinical model and is under investigation in human clinical trials(34,43,44). We observed a more marked Treg depletion in the highly cycling $CCR2^+$ subset following low-dose CP treatment in mice models. These results are consistent with previous observation that cycling Tregs having a phenotype associated with maximal suppression(45), are depleted by the same alkylating agent(46). Preferential $CCR2^+$ Treg eradication by low-dose cyclophosphamide in human

requires further investigations. CP sensitivity in vitro has also been associated with reduced detoxification processes due to lower intracellular ATP(47). We observed that $CCR2^+$ Tregs expressed higher level of the ecto-nucleoside triphosphate diphosphorylase CD39 which could contribute to the higher sensitivity of the subset. No preferential depletion of the $CD39^+CCR2^+$ Tregs was observed in vivo suggesting that CD39 expression does not predict CP sensitivity in contrast to cell cycle. Exogenous CCL2 addition neither enhanced Treg proliferation nor CP sensitivity in vitro (data not shown) suggesting that CCR2 exerts exclusively migratory function on Tregs. Preferential depletion of $CCR2^+$ Tregs after low-dose cyclophosphamide also occurred in the spontaneous MMTV-PyMT mammary carcinoma model. Beyond the weak and transient depletion of the overall Treg population, the preferential depletion of the $CCR2^+$ antigen-specific Treg subset might thus explain the strong combinatorial anti-tumor effect mediated by OTI cells adoptive transfer.

Our data demonstrate a crucial role of CCR2 in the regulation of Treg-mediated immunosuppression and provide more insights in the anti-tumor immune response after low-dose cyclophosphamide. These observations allowed us to define a novel target to improve the efficacy of chemotherapy.

Acknowledgments

The authors wish to thank, the Plateforme Imagerie Pitié-Salpêtrière (PICPS) for assistance with the two-photon microscope and the animal Facility “NAC” for mice breeding assistance.

References

1. Franciszkiewicz K, Boissonnas A, Boutet M, Combadiere C, Mami-Chouaib F. Role of chemokines and chemokine receptors in shaping the effector phase of the antitumor immune response. Cancer Res 2012;72(24):6325-32.
2. Chow MT, Luster AD. Chemokines in cancer. Cancer Immunol Res 2014;2(12):1125-31.
3. Shi C, Pamer EG. Monocyte recruitment during infection and inflammation. Nat Rev Immunol 2011;11(11):762-74.
4. Amoura Z, Combadiere C, Faure S, Parizot C, Miyara M, Raphael D, et al. Roles of CCR2 and CXCR3 in the T cell-mediated response occurring during lupus flares. Arthritis Rheum 2003;48(12):3487-96.
5. Carr MW, Roth SJ, Luther E, Rose SS, Springer TA. Monocyte chemoattractant protein 1 acts as a T-lymphocyte chemoattractant. Proc Natl Acad Sci U S A 1994;91(9):3652-6.
6. Galluzzi L, Buque A, Kepp O, Zitvogel L, Kroemer G. Immunological Effects of Conventional Chemotherapy and Targeted Anticancer Agents. Cancer Cell 2015;28(6):690-714.
7. Qian BZ, Li J, Zhang H, Kitamura T, Zhang J, Campion LR, et al. CCL2 recruits inflammatory monocytes to facilitate breast-tumour metastasis. Nature 2011;475(7355):222-5.
8. Conti I, Rollins BJ. CCL2 (monocyte chemoattractant protein-1) and cancer. Semin Cancer Biol 2004;14(3):149-54.
9. Darrasse-Jeze G, Podsypanina K. How numbers, nature, and immune status of foxp3(+) regulatory T-cells shape the early immunological events in tumor development. Front Immunol 2013;4:292.
10. Ondondo B, Jones E, Godkin A, Gallimore A. Home sweet home: the tumor microenvironment as a haven for regulatory T cells. Front Immunol 2013;4:197.
11. Curiel TJ. Tregs and rethinking cancer immunotherapy. J Clin Invest 2007;117(5):1167-74.
12. Shevach EM. Mechanisms of foxp3+ T regulatory cell-mediated suppression. Immunity 2009;30(5):636-45.
13. Munn DH, Mellor AL. The tumor-draining lymph node as an immune-privileged site. Immunol Rev 2006;213:146-58.
14. Wei S, Kryczek I, Zou W. Regulatory T-cell compartmentalization and trafficking. Blood 2006;108(2):426-31.
15. Campbell DJ, Koch MA. Phenotypical and functional specialization of FOXP3+ regulatory T cells. Nat Rev Immunol 2011;11(2):119-30.
16. Rubtsov YP, Niec RE, Josefowicz S, Li L, Darce J, Mathis D, et al. Stability of the regulatory T cell lineage in vivo. Science 2010;329(5999):1667-71.
17. Ding Y, Xu J, Bromberg JS. Regulatory T cell migration during an immune response. Trends Immunol 2012;33(4):174-80.
18. Lim HW, Broxmeyer HE, Kim CH. Regulation of trafficking receptor expression in human forkhead box P3+ regulatory T cells. J Immunol 2006;177(2):840-51.
19. Campbell DJ. Control of Regulatory T Cell Migration, Function, and Homeostasis. J Immunol 2015;195(6):2507-13.
20. Curiel TJ, Coukos G, Zou L, Alvarez X, Cheng P, Mottram P, et al. Specific recruitment of regulatory T cells in ovarian carcinoma fosters immune privilege and predicts reduced survival. Nat Med 2004;10(9):942-9.
21. Gobert M, Treilleux I, Bendriss-Vermare N, Bachelot T, Goddard-Leon S, Arfi V, et al. Regulatory T cells recruited through CCL22/CCR4 are selectively activated in lymphoid infiltrates surrounding primary breast tumors and lead to an adverse clinical outcome. Cancer Res 2009;69(5):2000-9.
22. Layseca-Espinosa E, Korniotis S, Montandon R, Gras C, Bouillie M, Gonzalez-Amaro R, et al. CCL22-producing CD8alpha- myeloid dendritic cells mediate regulatory T cell recruitment in response to G-CSF treatment. J Immunol 2013;191(5):2266-72.

23. Mitchell C, Couton D, Couty JP, Anson M, Crain AM, Bizet V, et al. Dual role of CCR2 in the constitution and the resolution of liver fibrosis in mice. Am J Pathol 2009;174(5):1766-75.
24. Bruhl H, Cihak J, Schneider MA, Plachy J, Rupp T, Wenzel I, et al. Dual role of CCR2 during initiation and progression of collagen-induced arthritis: evidence for regulatory activity of CCR2+ T cells. J Immunol 2004;172(2):890-8.
25. Zhang N, Schroppel B, Lal G, Jakubzick C, Mao X, Chen D, et al. Regulatory T cells sequentially migrate from inflamed tissues to draining lymph nodes to suppress the alloimmune response. Immunity 2009;30(3):458-69.
26. Hamano R, Baba T, Sasaki S, Tomaru U, Ishizu A, Kawano M, et al. Ag and IL-2 immune complexes efficiently expand Ag-specific Treg cells that migrate in response to chemokines and reduce localized immune responses. Eur J Immunol 2014;44(4):1005-15.
27. Engelhardt JJ, Boldajipour B, Beemiller P, Pandurangi P, Sorensen C, Werb Z, et al. Marginating dendritic cells of the tumor microenvironment cross-present tumor antigens and stably engage tumor-specific T cells. Cancer Cell 2012;21(3):402-17.
28. Saederup N, Cardona AE, Croft K, Mizutani M, Cotleur AC, Tsou CL, et al. Selective chemokine receptor usage by central nervous system myeloid cells in CCR2-red fluorescent protein knock-in mice. PLoS One 2010;5(10):e13693.
29. Zeelenberg IS, van Maren WW, Boissonnas A, Van Hout-Kuijer MA, Den Brok MH, Wagenaars JA, et al. Antigen localization controls T cell-mediated tumor immunity. J Immunol 2011;187(3):1281-8.
30. Boissonnas A, Scholer-Dahirel A, Simon-Blancal V, Pace L, Valet F, Kissenpfennig A, et al. Foxp3+ T cells induce perforin-dependent dendritic cell death in tumor-draining lymph nodes. Immunity 2010;32(2):266-78.
31. Boissonnas A, Licata F, Poupel L, Jacquelin S, Fetler L, Krumeich S, et al. CD8+ tumor-infiltrating T cells are trapped in the tumor-dendritic cell network. Neoplasia 2013;15(1):85-94.
32. Ford LB, Cerovic V, Milling SW, Graham GJ, Hansell CA, Nibbs RJ. Characterization of conventional and atypical receptors for the chemokine CCL2 on mouse leukocytes. J Immunol 2014;193(1):400-11.
33. Deaglio S, Dwyer KM, Gao W, Friedman D, Usheva A, Erat A, et al. Adenosine generation catalyzed by CD39 and CD73 expressed on regulatory T cells mediates immune suppression. J Exp Med 2007;204(6):1257-65.
34. Madondo MT, Quinn M, Plebanski M. Low dose cyclophosphamide: Mechanisms of T cell modulation. Cancer Treat Rev 2016;42:3-9.
35. Ghiringhelli F, Menard C, Puig PE, Ladoire S, Roux S, Martin F, et al. Metronomic cyclophosphamide regimen selectively depletes CD4+CD25+ regulatory T cells and restores T and NK effector functions in end stage cancer patients. Cancer Immunol Immunother 2007;56(5):641-8.
36. Brown CE, Vishwanath RP, Aguilar B, Starr R, Najbauer J, Aboody KS, et al. Tumor-derived chemokine MCP-1/CCL2 is sufficient for mediating tumor tropism of adoptively transferred T cells. J Immunol 2007;179(5):3332-41.
37. Fridlender ZG, Buchlis G, Kapoor V, Cheng G, Sun J, Singhal S, et al. CCL2 blockade augments cancer immunotherapy. Cancer Res 2010;70(1):109-18.
38. Guy CT, Cardiff RD, Muller WJ. Induction of mammary tumors by expression of polyomavirus middle T oncogene: a transgenic mouse model for metastatic disease. Mol Cell Biol 1992;12(3):954-61.
39. Bos PD, Plitas G, Rudra D, Lee SY, Rudensky AY. Transient regulatory T cell ablation deters oncogene-driven breast cancer and enhances radiotherapy. J Exp Med 2013;210(11):2435-66.
40. Drennan S, Stafford ND, Greenman J, Green VL. Increased frequency and suppressive activity of CD127(low/-) regulatory T cells in the peripheral circulation of patients with head and neck squamous cell carcinoma are associated with advanced stage and nodal involvement. Immunology 2013;140(3):335-43.

41. Lim KP, Chun NA, Ismail SM, Abraham MT, Yusoff MN, Zain RB, et al. CD4+CD25hiCD127low regulatory T cells are increased in oral squamous cell carcinoma patients. PLoS One 2014;9(8):e103975.
42. Schott AK, Pries R, Wollenberg B. Permanent up-regulation of regulatory T-lymphocytes in patients with head and neck cancer. Int J Mol Med 2010;26(1):67-75.
43. Le DT, Jaffee EM. Regulatory T-cell modulation using cyclophosphamide in vaccine approaches: a current perspective. Cancer Res 2012;72(14):3439-44.
44. Lutsiak ME, Semnani RT, De Pascalis R, Kashmiri SV, Schlom J, Sabzevari H. Inhibition of CD4(+)25+ T regulatory cell function implicated in enhanced immune response by low-dose cyclophosphamide. Blood 2005;105(7):2862-8.
45. Chen X, Subleski JJ, Kopf H, Howard OM, Mannel DN, Oppenheim JJ. Cutting edge: expression of TNFR2 defines a maximally suppressive subset of mouse CD4+CD25+FoxP3+ T regulatory cells: applicability to tumor-infiltrating T regulatory cells. J Immunol 2008;180(10):6467-71.
46. van der Most RG, Currie AJ, Mahendran S, Prosser A, Darabi A, Robinson BW, et al. Tumor eradication after cyclophosphamide depends on concurrent depletion of regulatory T cells: a role for cycling TNFR2-expressing effector-suppressor T cells in limiting effective chemotherapy. Cancer Immunol Immunother 2009;58(8):1219-28.
47. Zhao J, Cao Y, Lei Z, Yang Z, Zhang B, Huang B. Selective depletion of CD4+CD25+Foxp3+ regulatory T cells by low-dose cyclophosphamide is explained by reduced intracellular ATP levels. Cancer Res 2010;70(12):4850-8.

Figure Legends

Figure 1: CCR2 expression on Tregs is required for tumor-infiltration

(A) MCA-OVA tumor growth in WT mice (black round) or *Ccr2*$^{-/-}$ (white square). Graphs represent mean±SEM, (n=20 mice in each group, from three independent experiments). Two-way ANOVA with bonferoni's multiple-comparison test was used. (B) CCL2 protein level in supernatants of MCA-OVA cell cultures and (C) mice tumors (n=4-6 mice out of two experiments). ANOVA with bonferoni's multiple-comparison test was performed. (D) Quantification of the percentage of Treg among CD4^{+} cells in tumors (left) and dLN (right) of WT (black round) and *Ccr2*$^{-/-}$ mice (white square). Data represent mean±SEM of at least 10 mice from at least 3 independent experiments, Two-way ANOVA with bonferoni's multiple-comparison test was used.

(E) Parabiosis experimental protocol. (F) Representative dot plot showing Treg chimerism in dLN and tumors of mouse parabionts. (G) Graphs represent the proportion of WT and *Ccr2*$^{-/-}$ Tregs in dLN and tumors in WT (left) and *Ccr2*$^{-/-}$ parabionts (right). Two-way ANOVA with bonferoni's multiple-comparison used. (*p< 0.05,**p<0.01,***p<0.001).

Figure 2: CCR2^{+} Tregs accumulate during Tumor Development

CCR2 expression by Th and Treg were analyzed in (A) dLN, (B) Blood and (C) tumors. (Left panels), representative histograms plots showing CCL2-AF647 binding on Th and Tregs in WT (empty histograms) and *Ccr2*$^{-/-}$ mice (filled histograms). Graphs show mean±SEM of the percentage of CCR2^{+} cells (n= at least 9 mice in each group from three independent experiments). One-way ANOVA with bonferoni's multiple-comparison test was used to compare means at each time points with tumor free mice (D0) or with D7 in the tumor. (**p<0.01,***p<0.001).

Figure 3: CCR2$^+$ Tregs are activated, IL-10 producing and tumor-antigen specific cells

The phenotype of Ccr2$^+$ and Ccr2$^-$ Tregs was analysed on day 10 post tumor inoculation.

(A) Representative histograms plots of indicated surface markers .(B) Representative dot plot of IL-10 staining gated on dLN Treg subsets (left panel) and quantification (right panel). Data represent mean±SEM of 4 mice from 2 independent experiments. One-way ANOVA with bonferoni's multiple-comparison test was used. (C) Representative dot plots of concomitant CCR2 and DNA staining (Hoechst) (left panel) in dLN. Bars represent mean±SEM of 14 mice from 4 independent experiments (right panel). Student t-test was used. (D) Representative histogram plot of Ki-67 expression (left panel) in dLN. Bars represent mean±SEM of 6 mice from 2 independent experiments (right panel). Student t-test was used. (E) Representative histogram plots of CD73 and CD39 expression in dLN. Bars represent mean±SEM of 6 mice from 2 independent experiments. (F) Representative FACS dot plot of concomitant CCR2 and I-Ab $OVA_{323-339}$ tetramer staining in the dLN of tumor-free and tumor-bearing mice, percentage±SD are indicated (left panel). Quantification of CCR2$^+$ Treg in the tetramer negative and positive fraction (Tet- and Tet+), bars indicate mean±SEM (right panel) of 10 mice from 3 independent experiments. Student t-test was used. (*p<0.05,**p<0.01,***p<0.001).

Figure 4: CCR2$^+$ Tregs are preferentially depleted by low-dose cyclophosphamide treatment

(A) Graphs show percentage of dLN Treg among CD4$^+$ T cells in WT (left panel) and *Ccr2*$^{-/-}$ mice (right panel) treated (dashed lines) or not (full lines) with low-dose

cyclophosphamide (CP 100 mg/kg) on day 7. Data represent mean±SEM (n=6 to 10 mice from 2-5 independent experiments). (B) Quantification of the number of Treg $CCR2^+$ (left panel) and $CCR2^-$ (right panel) in WT mice. Data represent mean ±SEM (n=6 to 10 mice from 2-5 independent experiments). **(C)** Bars show the frequency of the indicated chemokine receptor among total Treg in the dLN on day 10. Data represent mean±SEM (n=5 mice per group). One-way Anova tests with Bonferroni's multiple comparison tests were used to compare treated to non-treated mice at each time points. **(D)** Bars represent the frequency of cycling ($Hoechst^+$, left panel and $Ki\text{-}67^+$, right panel) Tregs in the dLN on day 10. Data represent mean±SEM (n=5-8 mice per group, student t-tests was performed). (*p<0.05,**p<0.01,***p<0.001).

Figure 5: Low dose CP fails to enhance the priming of OT-1 in the dLN of *Ccr2*$^{-/-}$ mice

3 days after treatment with low-dose cyclophosphamide, CFSE-labeled OT-1 cells were transferred in tumor-bearing WT and *Ccr2*$^{-/-}$ mice. Proliferation and IFN-γ production of OT-1 in dLN were analyzed 3 days later. (A) Representative dot plots show CFSE dilution gated on $CD45.1^+$ OT-1 cells. (B) Quantification of OT-1 cell proliferation and INF-γ production on day 13. Data represent mean ±SEM (n= 15 mice from three independent experiments). (C) Tumor growth in CP-treated WT and *Ccr2*$^{-/-}$ mice with (white) or without (black) OT-1 adoptive transfer. Graphs represent mean±SEM of 15 to 20 mice in each group from 3 independent experiments. Two-way ANOVA with Bonferroni 's multiple comparison test was used. (*p<0.05,**p<0.01,***p<0.001).

Figure 6: CCR2$^+$ Tregs accumulate within spontaneous mammary carcinoma and are preferentially depleted by low-dose CP

(A) Representative contour plots (left panels) of CCL2 binding on Treg and Th cells from WT and *Ccr2*$^{-/-}$ MMTV-PyMT mice, 3 days after treatment with CP in (A) dLN (B) blood (C) tumor. Graphs show the percentage of CCR2$^+$ Tregs and Th (right panels). One-way ANOVA with Bonferroni's multiple comparison test was used (n=5 to 10 mice). (D) Graphs show correlative analysis between the percentage of CCR2$^+$ Tregs and the age at tumor onset in the blood (left panel) and the tumor (right panel). Linear regression was calculated and Pearson correlation coefficients are indicated. (*p<0.05,***p<0.001).

Figure 7: CCR2$^+$ Tregs accumulate within human OSCC

(A) Gating strategy for Th and Treg cells in human fresh blood (upper panels) and OSCC tumors (lower panels). Mean percentage±SD of Th and Treg among total CD4$^+$ cells in healthy control subjects (c) or OSCC patients (p) are indicated. Histogram plots show CCR2 expression on Tregs after pre-incubation with rhCCL2 competitor (grey histogram) or not (empty histogram). (B) Frequency of CCR2$^+$ Th and Tregs in the blood of healthy (n =42) or OSCC patients (n = 30) (left panels) and healthy gingival tissues (n = 10) or OSCC tumors (n = 14) (right panels). Two-tailed Mann Whitney test was used (p-values are indicated).

Supplementary Methods

Multiphoton imaging

All imaging experiments were performed on explanted tissue. LNs were carefully collected and were immobilized in an imaging chamber perfused with oxygenated (95% O_2 plus 5% CO_2) RPMI medium containing 10% FCS. Local temperature was monitored and maintained at 37°C. Lymph node imaging was performed 10 days after tumor inoculation. T cells could be detected up to 200 µm from the surface of LNs. Measurements were performed in at least three independent experiments.

The two-photon laser scanning microscopy (TPLSM) setup used was a Zeiss LSM 710 NLO multiphoton microscope (Carl Zeiss, Le Pecq, France) coupled to a Ti/sapphire crystal laser (Coherent Chameleon Ultra , Santa Clara, CA) that provides 140-fs pulses of near-infrared (NIR) light, selectively tunable between 680 and 1080 nm, and an acousto-optic modulator to control laser power.GFP was detected using two-dichroic mirrors (495 nm and 555 nm) with 520/35 bandpass filter. The excitation wavelength was 870 nm. Cell motility was measured every 30 seconds by 9 consecutive 5-µm z spacing stacks using a plan apochromat ×20 (NA = 1) water immersion objective. Fluorescent cells were monitored over time with three-dimensional automatic tracking and manual correction with Imaris software (Bitplane). The acquisition and analysis protocols for all experimental conditions to be compared were identical. The arrest coefficient was defined as the proportion of time each cell's instantaneous velocity (calculated for every 30 s interval) was less than 2 µm/min.

Antibodies

The following panel of anti-mouse surface antibodies was used: anti-CD4 (clone RM4-5), anti-CD3(clone 145-2C11), anti-CD25 (clone PC61), anti-Ly6c (clone AL-21), anti-CD44 (clone IM7), anti-CD62L (clone MEL-14), anti-CD69 (clone H1-2F3), anti-CD45.1 (clone A20), anti-CD11b (clone M1/70), anti-*I-A*(*b*) (clone AF6-120-1),

anti-CD11c (clone HL3), anti-CD45 (clone 30-F11), anti-IFNγ (clone XMG1.2), anti-CCR4 (clone 2G12), anti-CCR5 (clone 2D7), anti-CCR6 (clone 11A9),anti-CD16/32 (2.4G2; BD Biosciences), anti-CD64 (clone X54-5/7.1.1), anti-IL-10 (clone JES5-16E3), anti-CD39 (clone A1) (BioLegend, San Diego, CA, USA) ,anti-CCR2 (clone 475301;R&D systems), anti-CD73 (clone TY/11.8;eBioscience) .

The following panel of anti-human surface antibodies was used: anti-CD4 (clone VIT4), anti-CD25 (clone 4E3), anti-CD127 (clone MB15-18C9) (Miltenyi Biotec), anti-Foxp3 (clone 236A/E7; eBioscience), anti-CD45 (clone H130; BD Pharmigen) and anti-CCR2 (clone KO36C2; Biolegend).

Supplemental figure 1: Tregs fail to migrate to the tumor in Ccr2$^{-/-}$ mice but accumulate in the dLN

(A) Flow cytometric identification of Treg ($CD4^+CD3^+CD25^+Foxp3^+$) and Th ($CD4^+CD3^+CD25^-Foxp3^-$) subsets in the tumor and in the dLN at day 10 post tumor inoculation.

Quantification of the number of Treg (B-D) and Th (C-E) in tumors and dLNs of WT (black circles) and Ccr2$^{-/-}$ mice (white squares) at different time points post tumor inoculation. Data are representative of at least 10 mice in each group from at least 3 independent experiments. Two-way ANOVA with bonferoni's multiple-comparison test was used to compares means from WT and Ccr2$^{-/-}$ mice at each time points. (**p<0.01; ***p<0.001).

Supplemental figure 2: The dynamic of Treg is reduced in the dLN of Ccr2$^{-/-}$ mice compared to WT mice

ELISA detection of the CCL2 protein level in (A) dLN and (B) plasma at different time point following tumor inoculation of MCA-OVA or in tumor-free mice (TF). Bars represent means ±SEM of 8 mice in each group from two independent experiment. ANOVA with bonferoni's multiple-comparison test was performed.

(C) The dynamic of Tregs was analyzed by time-lapse two photon imaging of explanted LNs at day 10 post tumor innoculation in Foxp3-GFP mice. Representative images show typical Treg (green) track paths over time (red line). (D) Quantification of mean speed of Tregs in dLN and non-dLN. Median are indicated (red bars). Data are pooled from different movies out of three independent experiments. n=335 Treg for dLN of WT mice; n=340 for dLN of Ccr2$^{-/-}$ mice; n=90 for non-dLN of WT mice; n=106 for non-dLN of Ccr2$^{-/-}$ mice. One-way ANOVA with bonferoni's multiple-comparison test

was used. (E) Graph shows the distribution of arrest coefficients of Tregs in WT and Ccr2$^{-/-}$ mice in dLN at D10 after tumor inoculation. Mann-Whitney non-parametric t test was performed. Symbol used *** P<0.001. Scale bar: 25 µm

(F) FACS dot plots show the gating strategy for the different APC subsets in the dLN at D10. (G) Mean ± SEM of each indicated subset in the dLN of tumor free mice or WT and Ccr2$^{-/-}$ mice, 10 days after tumor inoculation. Data are representative of 4 mice in each group from two independent experiments. Two-way ANOVA with Bonferroni's for multiple comparison test was used. (*p< 0.05,***p<0.001).

Supplemental Figure 3: CCL2-AF647 staining allows specific characterization of CCR2 receptor expression on Treg cells

(A) Representative histograms plots of anti-CCR2 antibody staining on blood inflammatory monocytes (CD11b^{+}Ly6c^{high}) and Tregs (Upper panels) and CCL2-AF647 binding (Lower panels) in WT and Ccr2$^{-/-}$ tumor free mice.(B) Representative histograms plots of CCL2-AF647 binding inhibition on dLN Treg and Th using unlabelled rhCCL2 at day 8 post tumor innoculation. (C) Representative histograms plots of CCL2-AF647 binding on Tregs in the Blood, dLN, and tumor at day 10 post tumor innoculation in relevant chemokine receptor deficient mice compared to Ccr2$^{-/-}$ mice. Data are representative of 3 mice per groups. (D) Representative contour plots showing the expression of the *Ccr2*-transcriptional red fluorescent reporter (RFP) and CCL2-binding on dLN Tregs of tumor-bearing indicated mouse strains. Bars represent mean ±SEM of 8 mice from 3 independent experiments. (E) Representative dot plot showing the co-selection of CCR2^{+} Tregs with the indicated chemokine receptors in the dLN and the tumor, 10 days after tumor inoculation. Percent ±SD from 5 different mice are indicated for each quadrant. Left graphs show the proportion of each CCR

among $CCR2^+$ Tregs. Right graphs show the proportion of $CCR2^+$ Treg in each CCR+ Treg subsets. Data are mean ±SEM of 5 different mice.

Supplemental figure 4: Non-cycling Tregs accumulate in the dLN of $Ccr2^{-/-}$ mice compare to WT mice

(A) Representative histogram plots of DNA staining (hoechst) at day 8 post tumor inoculation, in Treg (upper panels) and Th (lower panels) in WT (white histograms) and $Ccr2^{-/-}$ (grey histograms). Percent of cell in S G2/M phases are indicated. (B) The percent (left panels) and absolute numbers (right panels) of cycling Treg and Th from WT (white bars) and $Ccr2^{-/-}$ (grey bars) mice were analyzed at day 8 and 13 post tumor inoculation. Bars represent mean ± SEM (n= 9 mice from three independent experiments at day 8 and n= 4 mice out of 2 experiments at day 13 post tumor inoculation). One-way ANOVA with Bonferroni‘s multiple comparison test was used for statistical analysis. (**p< 0.01).

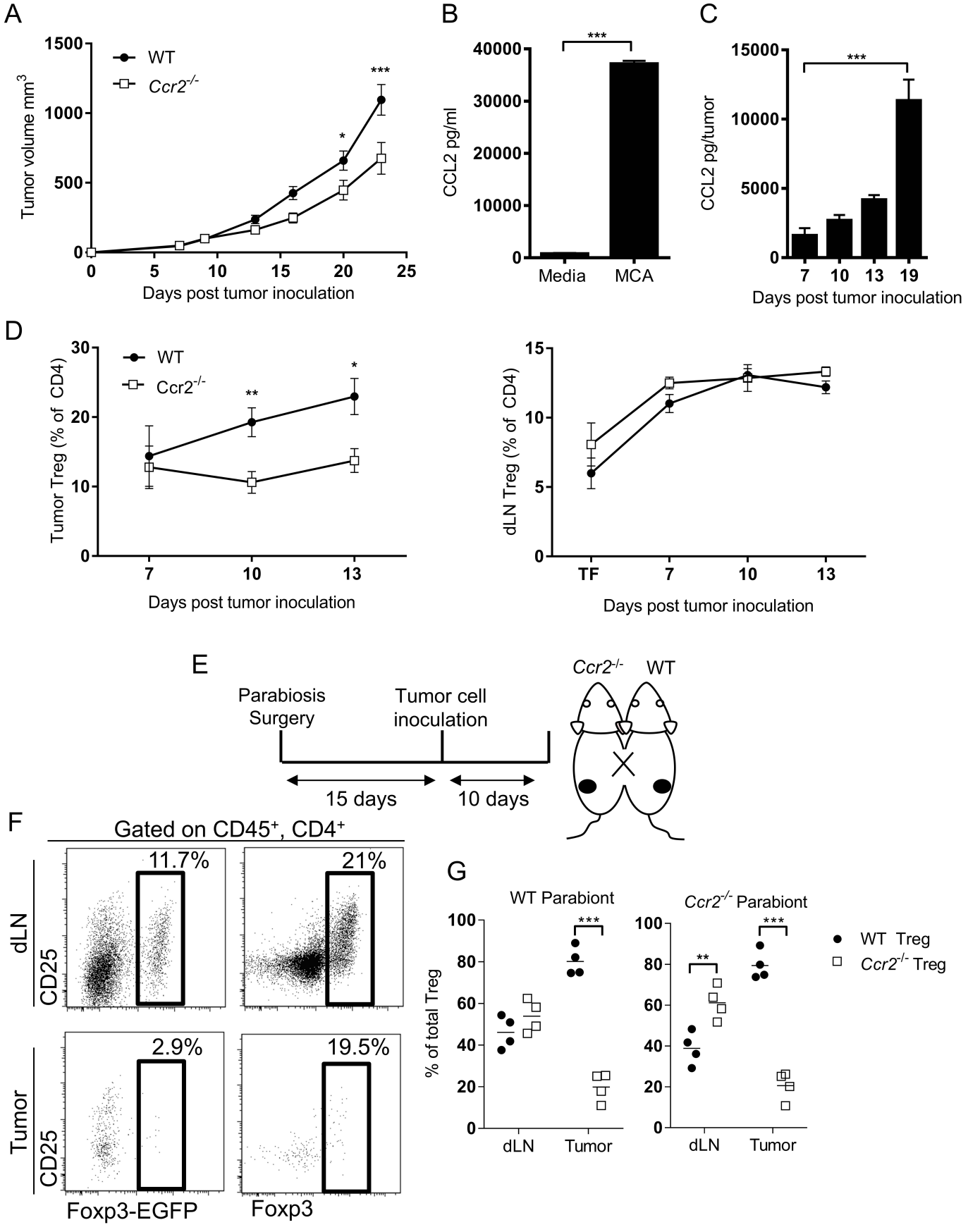

Figure 1: CCR2 expression on Tregs is required for tumor-infiltration

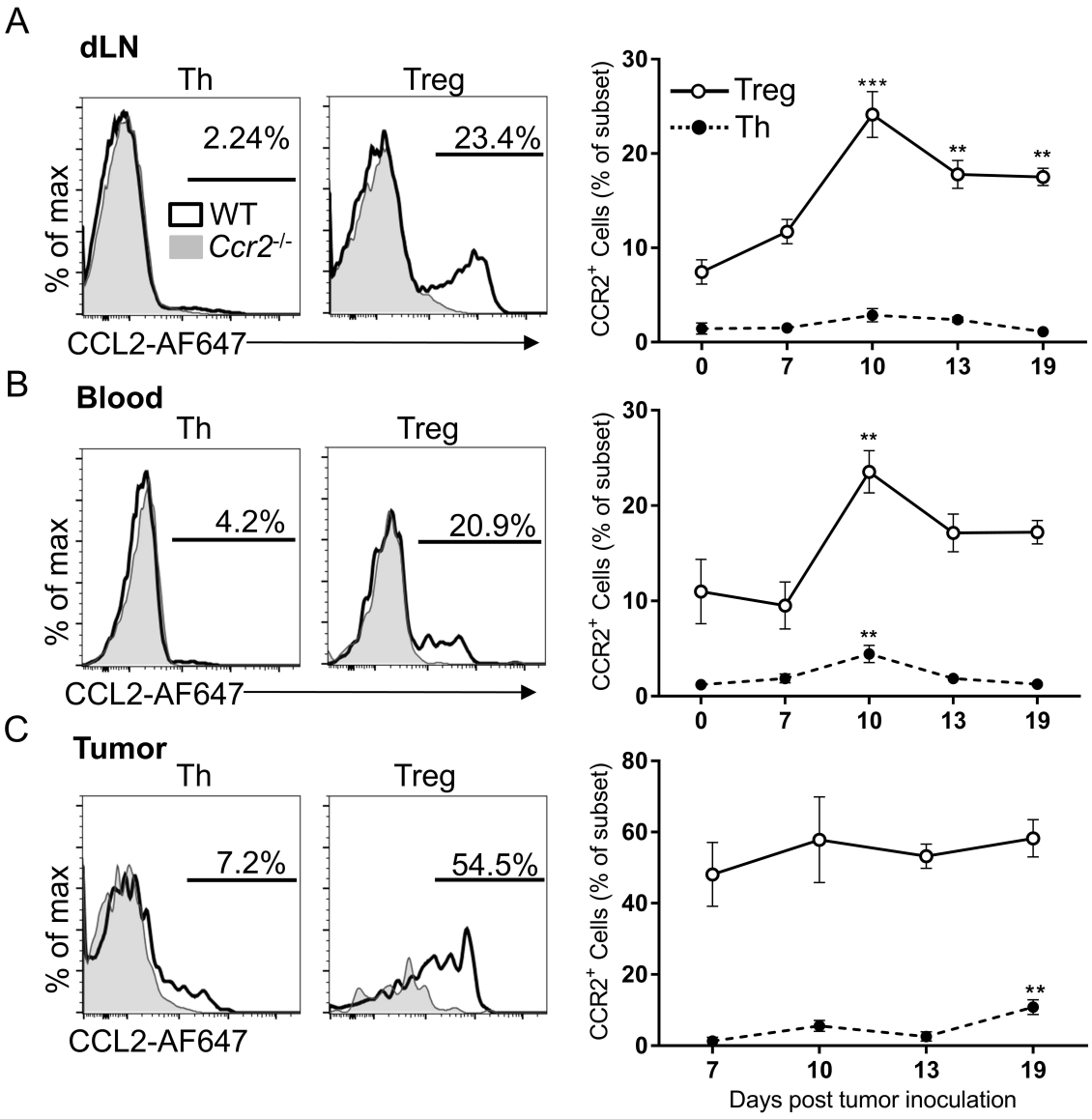

Figure 2: CCR2⁺ Tregs accumulate during Tumor Development

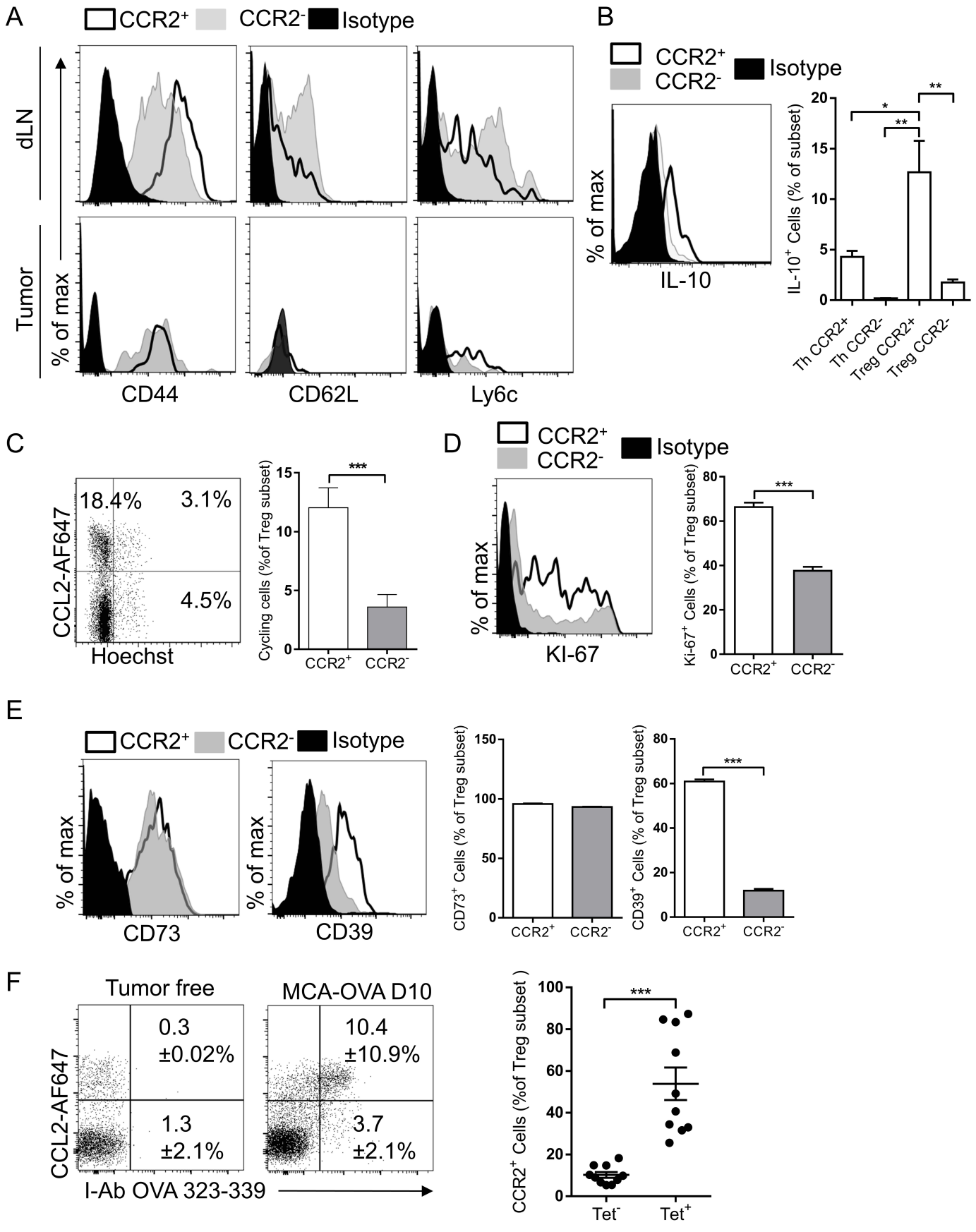

Figure 3: CCR2+ Tregs are activated, IL-10 producing and tumor-antigen specific cells

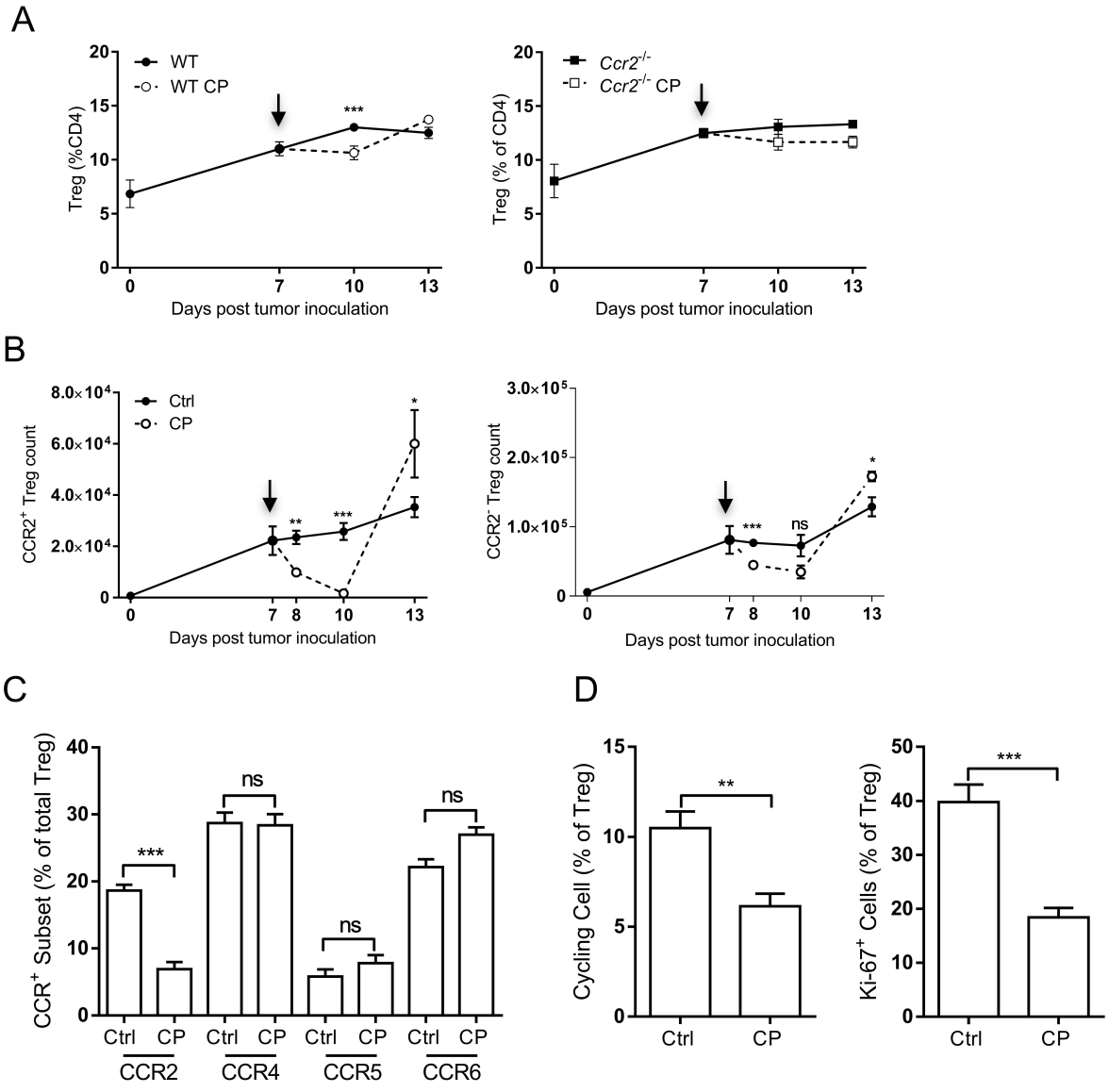

Figure 4: CCR2⁺ Tregs are preferentially depleted by low-dose cyclophosphamide treatment

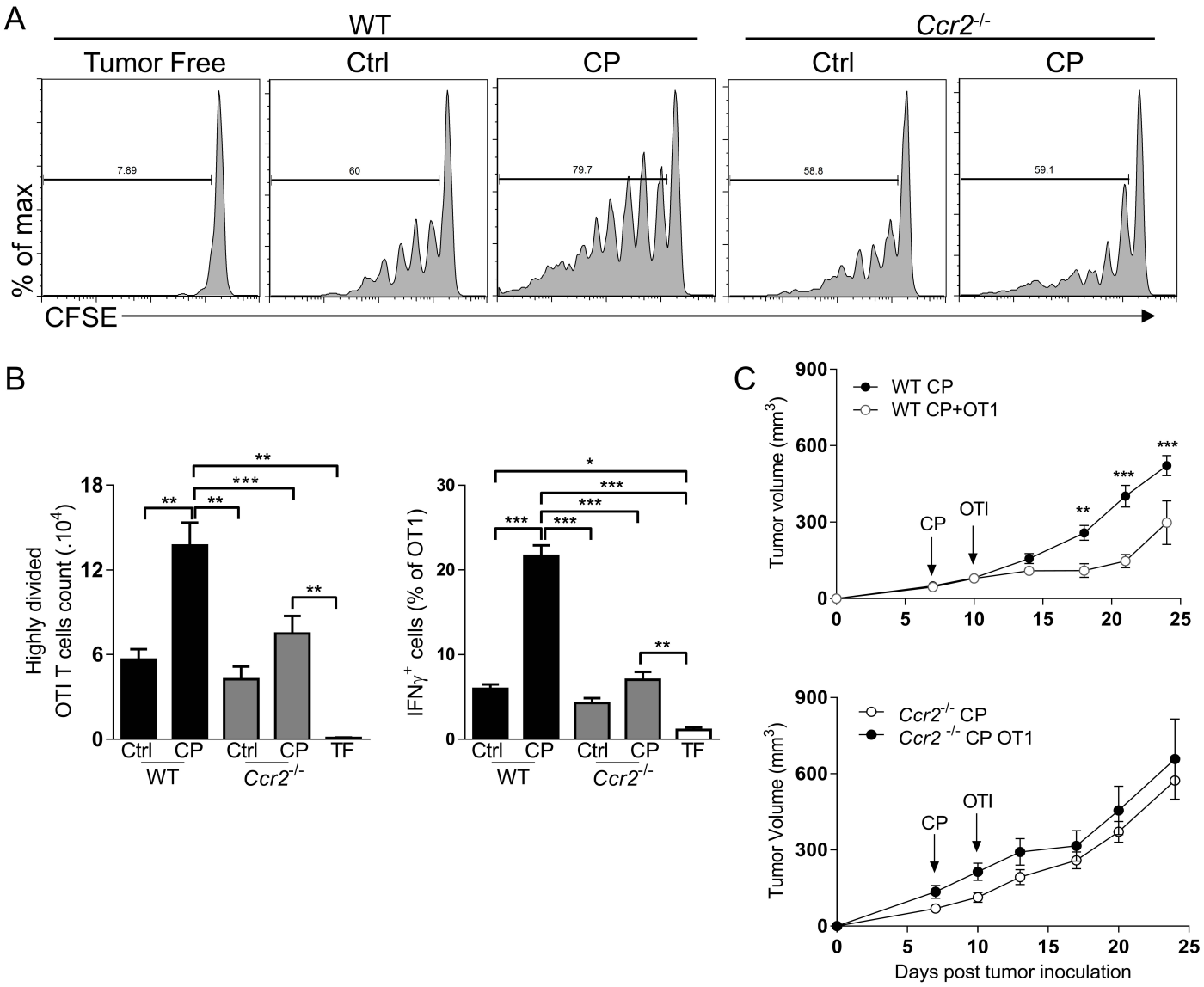

Figure 5: Low-dose CP fails to enhance the priming of OT-1 in the dLN of Ccr2$^{-/-}$ mice

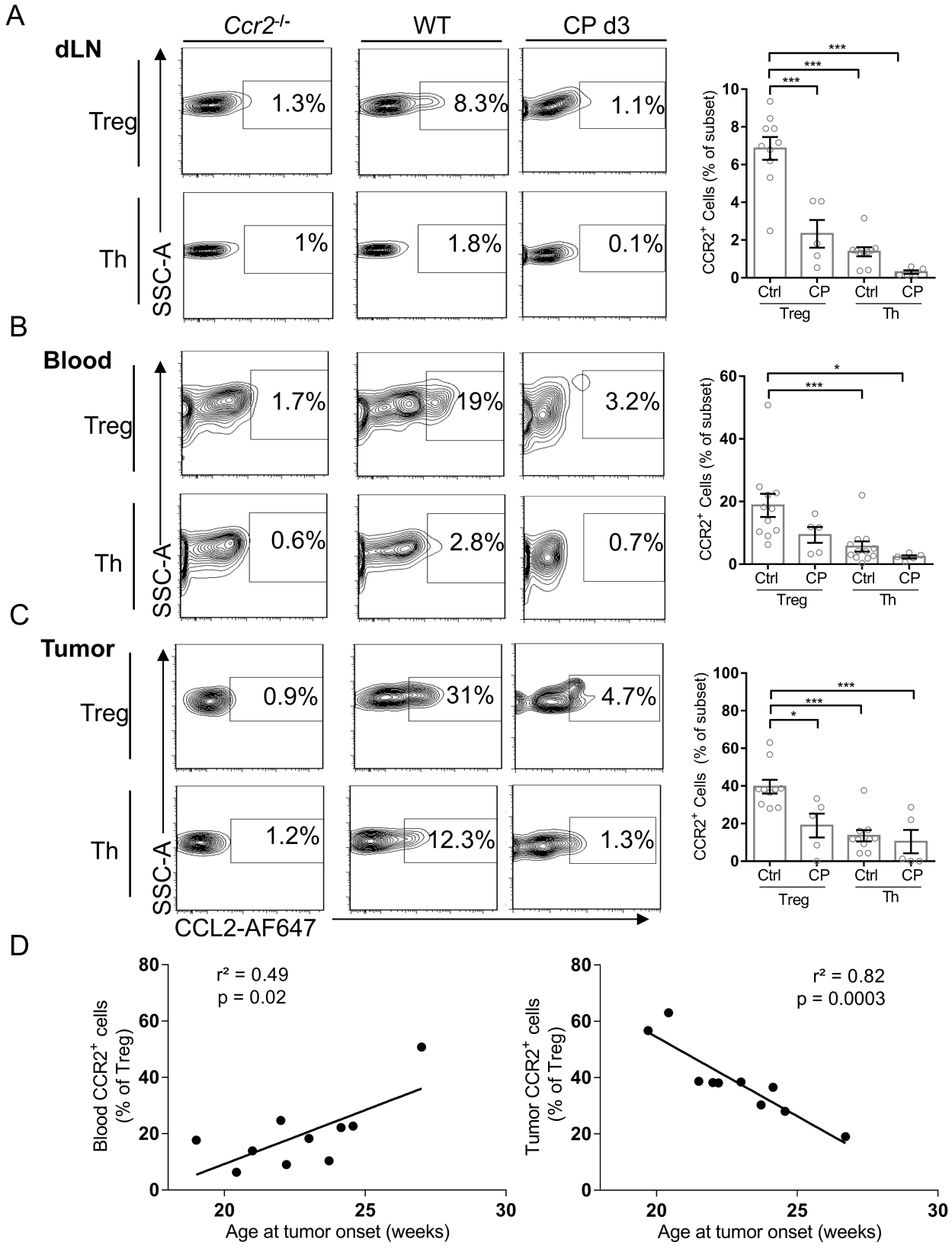

Figure 6: CCR2⁺ Tregs accumulate within spontaneous mammary carcinoma and are preferentially depleted by low-dose CP

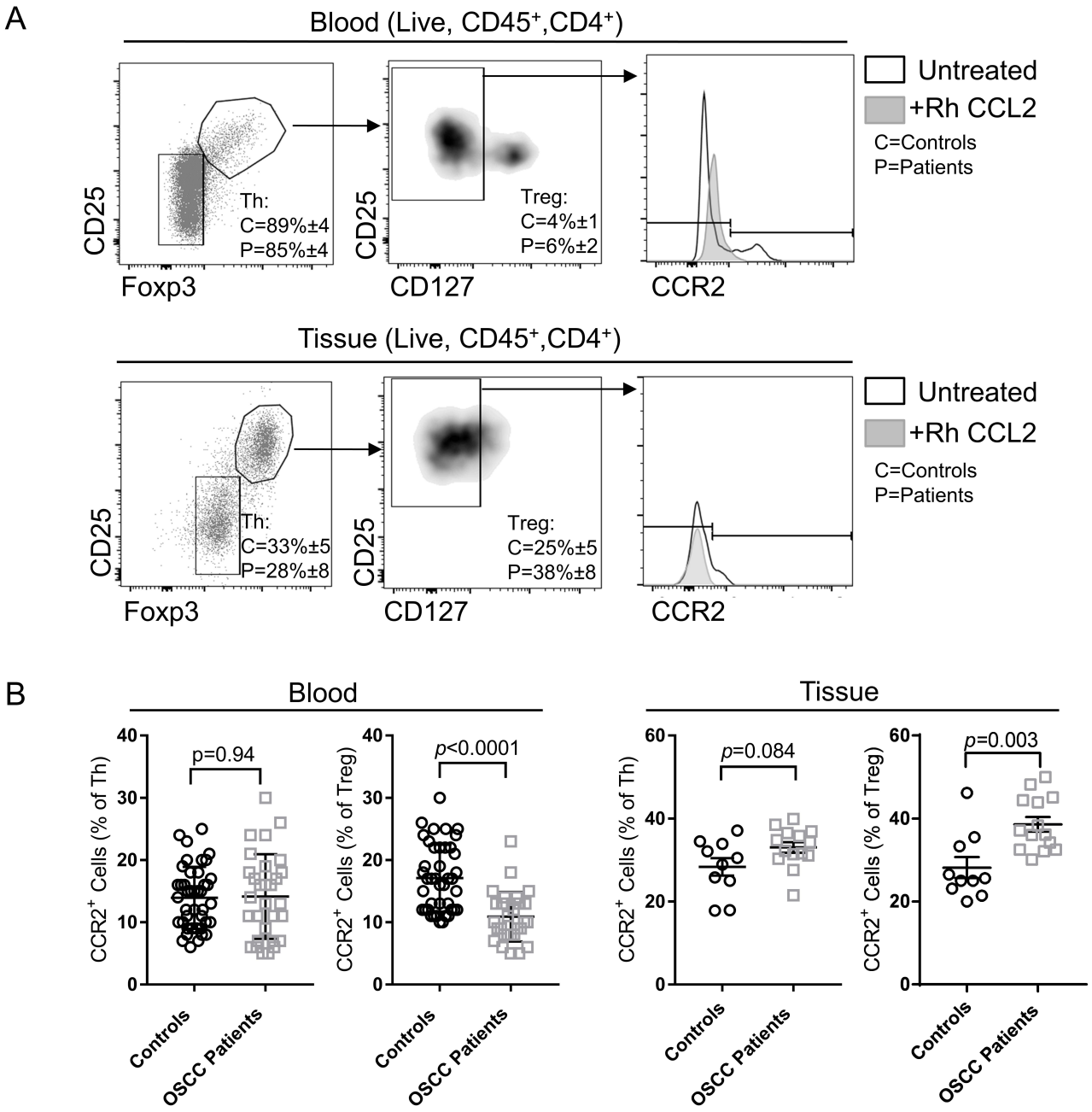

Figure 7: CCR2⁺ Tregs accumulate within human OSCC

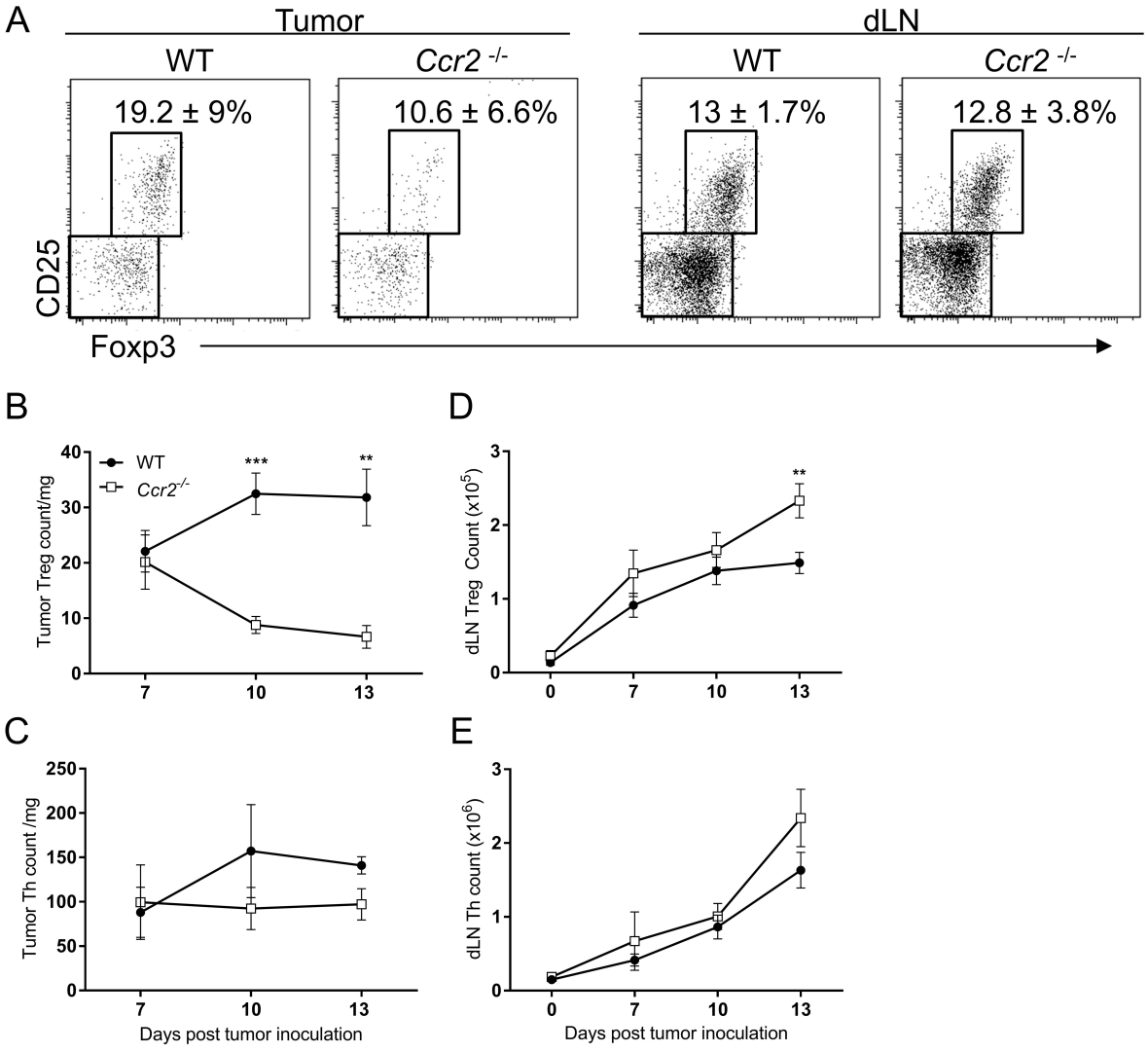

Supplemental figure 1: Tregs fail to migrate to the tumor in Ccr2$^{-/-}$ mice but accumulate in the dLN

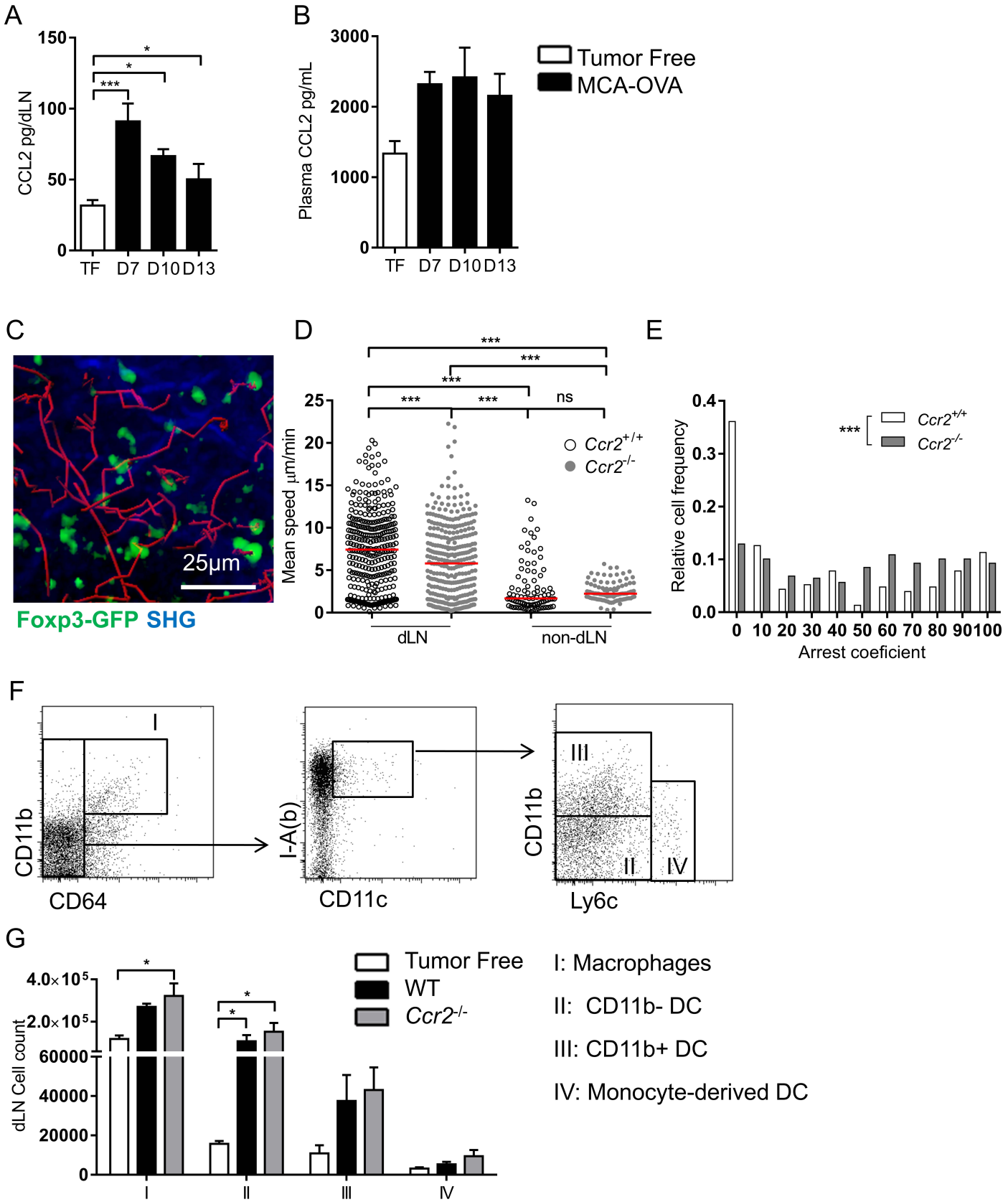

Supplemental Figure 2: The dynamic of Tregs is reduced in the dLN of *Ccr2*$^{-/-}$ mice compared to WT mice

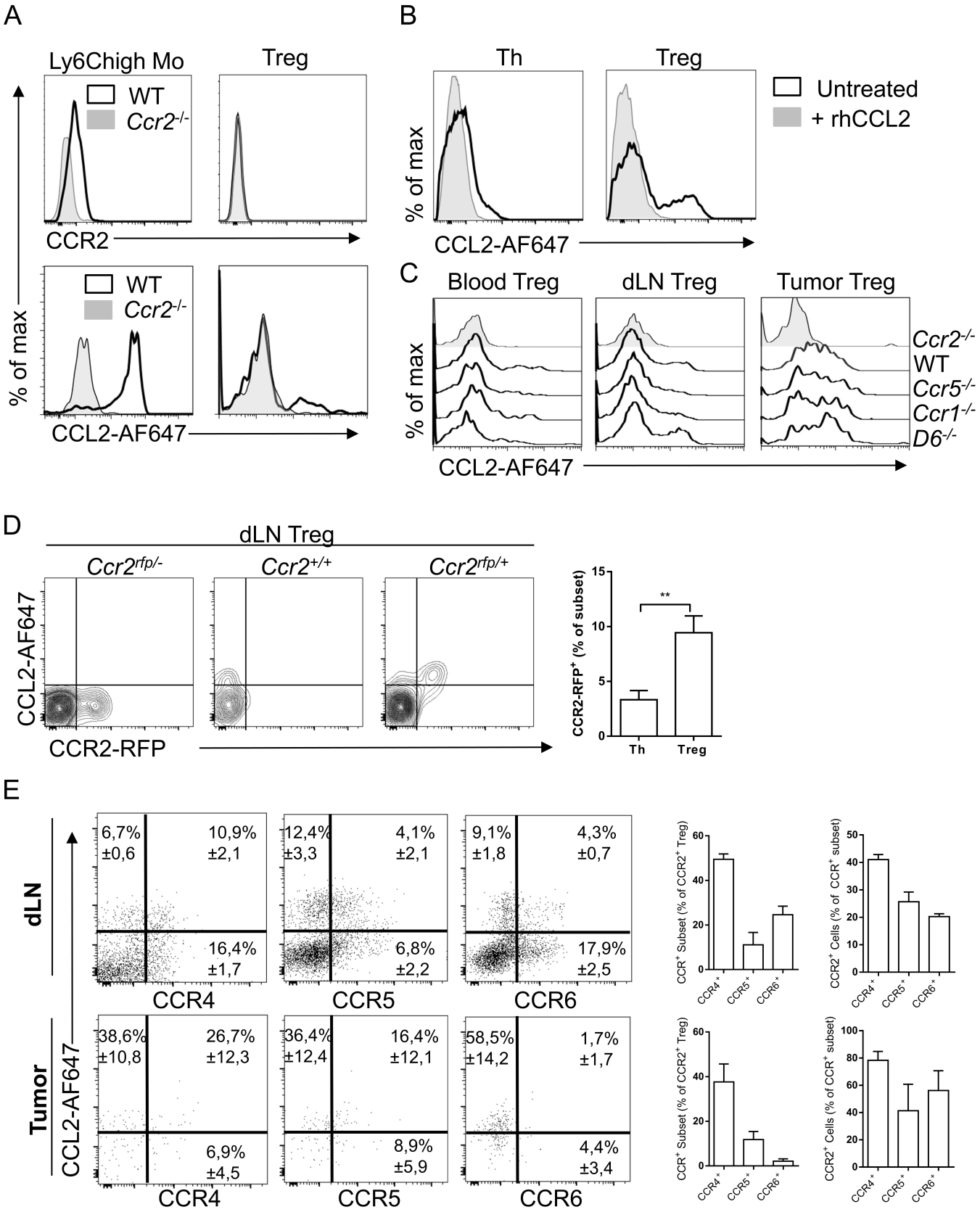

Supplemental Figure 3: CCL2-AF647 staining allows specific characterization of CCR2 receptor expression on Tregs

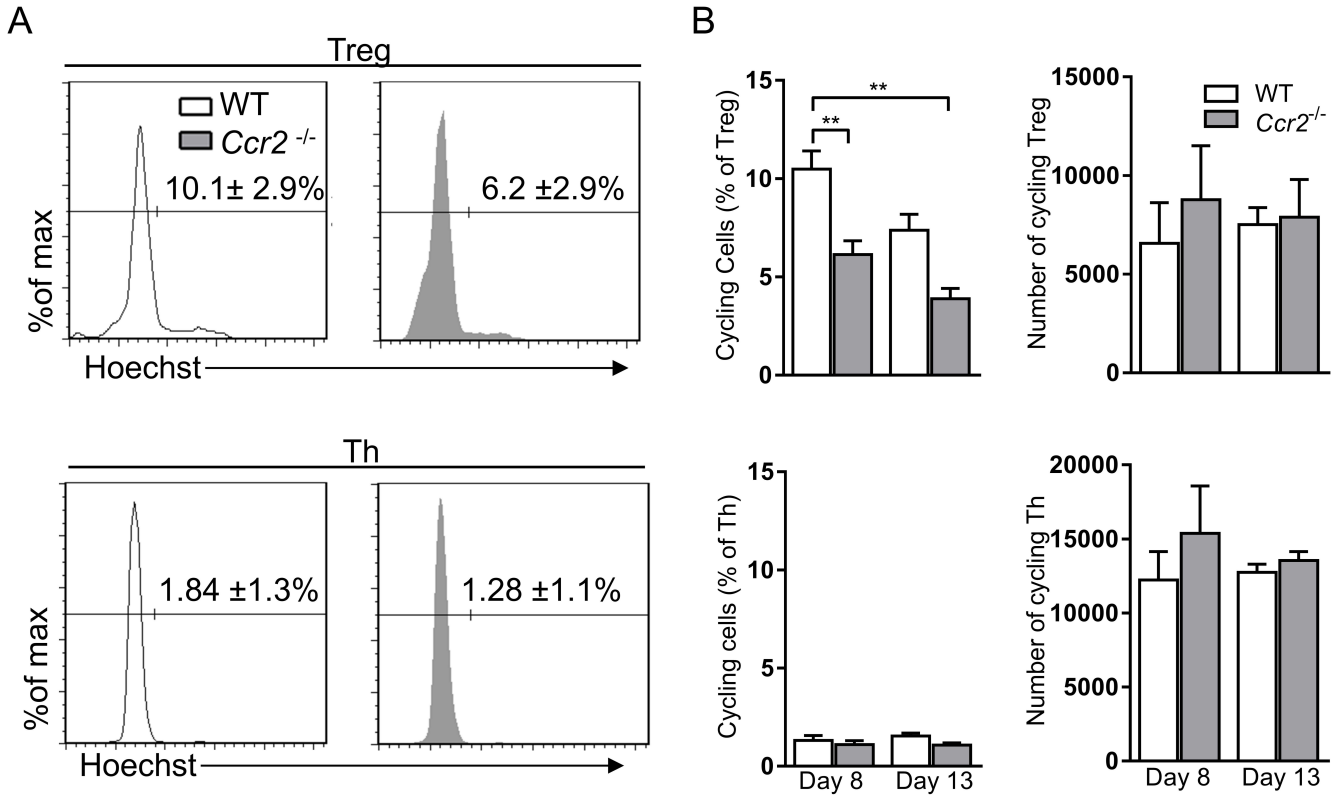

Supplemental figure 4: Non-cycling Tregs accumulate in the dLN of Ccr2$^{-/-}$ mice compare to WT mice